The Role of Linear Interference in Northern Annular Mode Variability Associated with Eurasian Snow Cover Extent

KAREN L. SMITH AND PAUL J. KUSHNER

Department of Physics, University of Toronto, Toronto, Ontario, Canada

JUDAH COHEN

Atmospheric and Environmental Research, Inc., Lexington, Massachusetts

(Manuscript received 20 January 2011, in final form 8 June 2011)

ABSTRACT

One of the outstanding questions regarding the observed relationship between October Eurasian snow cover anomalies and the boreal winter northern annular mode (NAM) is what causes the multiple-week lag between positive Eurasian snow cover anomalies in October and the associated peak in Rossby wave activity flux from the troposphere to the stratosphere in December. This study explores the following hypothesis about this lag: in order to achieve amplification of the wave activity, the vertically propagating Rossby wave train associated with the snow cover anomaly must reinforce the climatological stationary wave, which corresponds to *constructive linear interference* between the anomalous wave and the climatological wave. It is shown that the lag in peak wave activity flux arises because the Rossby wave train associated with the snow cover is in quadrature or out of phase with the climatological stationary wave from October to mid-November. Beginning in mid-November the associated wave anomaly migrates into a position that is in phase with the climatological wave, leading to constructive interference and anomalously positive upward wave activity fluxes until mid-January. Climate models from the Coupled Model Intercomparison Project 3 (CMIP3) do not capture this behavior. This linear interference effect is not only associated with stratospheric variability related to Eurasian snow cover anomalies but is a general feature of Northern Hemisphere troposphere–stratosphere interactions and, in particular, dominated the negative NAM events of the fall–winter of 2009/10.

1. Introduction

It is well established that the observational record reveals a statistically significant relationship between autumnal Eurasian snow cover anomalies and Northern Hemisphere wintertime extratropical circulation anomalies (Watanabe and Nitta 1998; Cohen and Entekhabi 1999; Cohen et al. 2007). In years when there is anomalously high snow cover in Eurasia in October, the subsequent wintertime circulation pattern projects onto the negative phase of the northern annular mode (NAM; Thompson and Wallace 2000; Cohen et al. 2010). Consequently, when Eurasian snow cover is included as a predictor in statistical forecasts, the wintertime surface temperature forecast skill, much of which is NAM related, improves over much of the Northern Hemisphere (Foster et al. 1983; Cohen and Fletcher 2007; Orsolini and Kvamsto 2009). In observations, October Eurasian snow extent is associated with a vertically propagating Rossby wave train and correlates positively with December vertical wave activity flux into the stratosphere (Cohen et al. 2007; Hardiman et al. 2008).

Previous modeling work has helped improve our dynamical understanding of this snow–circulation connection (Gong et al. 2002, 2003; Fletcher et al. 2009; Orsolini and Kvamsto 2009; Smith et al. 2010; Allen and Zender 2010). However, our understanding is far from complete, and an important question remains regarding the timing: what accounts for the multiple-week lag between Eurasian snow cover anomalies in October and the associated peak wave activity flux in December? At the surface, anomalously large autumnal snow cover extent in Eurasia during October leads to colder local temperatures in Eurasia in the subsequent winter, by enhancing cold-air intrusions (Foster et al. 1983; Vavrus

Corresponding author address: Karen L. Smith, Dept. of Physics, University of Toronto, 60 St. George St., Toronto, ON M5S 1A7, Canada.
E-mail: ksmith@atmosp.physics.utoronto.ca

DOI: 10.1175/JCLI-D-11-00055.1

2007). The shallow layer of air overlying snow cover is colder than the surrounding air, primarily due to the increase in surface albedo (Wagner 1973; Mote 2008). When high-latitude Eurasia October snow cover is early and more extensive, anomalously cold surface temperatures enhance the formation of the Siberian high. Anticyclonic flow advects cold air southward, cooling the continent in fall and winter. Early development of the Siberian high prevents incursions of maritime air in autumn and topographic features in the region limit warm-air advection from the south. By December the Siberian high is strong enough to prevent interior temperatures from rising above freezing, keeping the snow cover relatively constant throughout the winter months. But this localized surface circulation response does not explain the hemispheric-scale and vertically deep connection between October snow and the wintertime NAM (Thompson and Wallace 1998). Our primary aim in this study is to address this question with an observational analysis that focuses on the structure and phase of the Rossby waves associated with October Eurasian snow cover anomalies.

Vertical fluxes of Rossby wave activity (Eliassen–Palm or EP fluxes) from the troposphere to the stratosphere (represented by upper-tropospheric and lower-stratospheric meridional eddy heat fluxes) correlate strongly negatively with the NAM index in the stratosphere and subsequently in the troposphere (Newman et al. 2001; Polvani and Waugh 2004). Garfinkel et al. (2010) have shown that stratospheric NAM variability is negatively correlated with the amplitude of the wave pattern that corresponds to the climatological stationary wave field, particularly its wave-1 and -2 components (see also Kolstad and Charlton-Perez 2010). They find that when the climatological stationary wave field is amplified or attenuated, the stratospheric jet correspondingly weakens or strengthens. Using multiple linear regression, Garfinkel et al. (2010) also demonstrated that the influence of October Eurasian snow cover on the polar stratosphere is in part associated with specific tropospheric wave patterns in December, including an eastern European high and a northwestern Pacific low. These wave patterns amplify the climatological stationary wave field and, consequently, the wave activity flux into the stratosphere. While this result is consistent with earlier studies (Cohen et al. 2007; Hardiman et al. 2008; Orsolini and Kvamsto 2009), the question of the multiple-week lag between October snow cover anomalies and the wintertime NAM remains.

Smith et al. (2010) describe the Garfinkel et al. results in terms of *linear interference* between wave anomalies and the climatological stationary wave. In general circulation model (GCM) integrations in which snow forcing and surface cooling are prescribed, Smith et al. find that in order to achieve amplification of the wave activity into the stratosphere, the forced wave must constructively interfere with the preexisting climatological stationary wave. This effect, which corresponds to wave activity flux contributions that scale linearly with the forced wave amplitude, dominates over nonlinear contributions for sufficiently weak forcing. The effect helps to explain the transient dynamics of snow-forced simulations of a comprehensive GCM and the sensitivity to different configurations of surface cooling in a suite of simplified GCM integrations. Similar relationships between the wave field and the NAM have been highlighted by Ineson and Scaife (2009) and Fletcher and Kushner (2011) with respect to GCM simulations with prescribed ENSO forcing, and by Martius et al. (2009), Woollings et al. (2010), and Nishii et al. (2010) with respect to blocking.

Expanding on the modeling analysis in Smith et al. (2010), we here address the observed lag between October Eurasian snow cover and the boreal winter NAM anomaly. After describing the methods and data used (section 2), we first establish the potential importance of linear interference effects by showing that wintertime coupled stratosphere–troposphere NAM variability is generally controlled by terms in the wave activity flux that are linear in the interannual wave anomalies (section 3a). We then show that the wave anomaly associated with snow cover that develops in fall is initially out of phase with the climatological wave and later moves into phase with the climatological wave (section 3b). Thus, the delay in stratospheric wave activity flux can be attributed to initially unfavorable interference conditions between the Rossby wave train associated with the snow cover anomalies and the climatological stationary wave. Although the reasons for the phase shift remain unclear, this analysis highlights the key role of linear interference in contributing to polar stratospheric variability. In section 3c, we show how this diagnostic approach applies to case studies of individual seasons. In particular, we present a case study of the strong negative NAM events of fall–winter 2009/10 (Cohen et al. 2010) within the context of linear interference.

Another aim of this study is to revisit the issue of the inability of current climate models to capture the observed snow–circulation connection (Hardiman et al. 2008). Hardiman et al. (2008) find that the suite of Coupled Model Intercomparison Project 3 (CMIP3) models does not show the NAM-like correlation between October snow cover and the wintertime circulation. Hardiman et al. (2008) propose a variety of reasons for this, for example related to the longitudinal scale of the anomalous waves associated with October Eurasian snow cover anomalies. As in observations, in GCMs the linear interference effect dominates wave-driven NAM variability; we find that the representation of the linear

interference effect coherent with snow is not accurately captured in the models, contributing to their unrealistic behavior (section 3d).

2. Methods

We analyze the relationship between Eurasian snow cover and the atmospheric circulation for the September–February season for the years 1972–2009. Meteorological observations are derived from the daily averaged National Centers for Environmental Prediction–National Center for Atmospheric Research (NCEP–NCAR) reanalysis dataset (Kalnay et al. 1996). The October Eurasian snow index (OCTSNW) is a standardized snow cover anomaly index generated from the Rutgers Eurasian snow cover extent time series (Robinson et al. 1993; information online at http://climate.rutgers.edu/snowcover). In addition, we use the twentieth-century simulations (20C3M), with corresponding radiative forcing, of the coupled ocean–atmosphere GCMs from the CMIP3 (information online at http://www.pcmdi.llnl.gov/projects/cmip/index.php). The length of these simulations varies from 100 to 150 yr. Linear trends have been removed from all time series. We carry out correlation and regression analysis between the annual OCTSNW index and various atmospheric fields (Wilks 2006) through the daily evolution of the fall-to-winter season. The atmospheric fields that we focus on are the geopotential height (GPH) area averaged over the polar cap bounded by 60°N, denoted Z_{pcap}, which corresponds to the NAM (Cohen et al. 2002; Baldwin and Thompson 2009); the eddy GPH at 60°N, Z^* (where the superscript asterisk indicates the deviation from the zonal mean); and the zonal mean meridional eddy heat flux averaged from 40° to 80°N, $\{v^*T^*\}$ (braces indicating a zonal mean), which corresponds to the vertical component of the wave activity flux.

Smith et al.'s (2010) modeling study developed a decomposition of the wave activity flux response that distinguished terms that were linear and nonlinear in the forced wave response to surface diabatic cooling. Here, we employ an analogous decomposition for the interannual variability of the wave activity flux (see also Nishii et al. 2009). We define, for a given day during year j,

$$v_j^* = v_j^{*\prime} + v_c^* \quad \text{and} \quad T_j^* = T_j^{*\prime} + T_c^*, \tag{1}$$

where the prime indicates the deviation from the climatological time mean (i.e., the anomaly), the subscript j indicates the year, and the subscript c indicates the climatological mean. Using v_j^* and T_j^* from (1), we can then find the anomalous eddy heat flux at that time in year j, $\{v^*T^*\}_j' = \{v_j^*T_j^*\}'$, as follows:

$$\begin{aligned}\{v_j^*T_j^*\}' &= \{v_j^*T_j^*\} - \{v_j^*T_j^*\}_c \\ &= \{v_j^{*\prime}T_j^*\} + \{v_j^{*\prime}T_c^*\} + \{v_c^*T_j^{*\prime}\} + \{v_c^*T_c^*\} - \{v_j^*T_j^*\}_c \\ &= \{v_j^{*\prime}T_j^{*\prime}\} + \{v_j^{*\prime}T_c^*\} + \{v_c^*T_j^{*\prime}\} + \{v_c^*T_c^*\} - \{v_c^*T_c^*\} - \{v_j^{*\prime}T_j^{*\prime}\}_c \\ &= \text{NONLIN} + \text{LIN}, \end{aligned} \tag{2}$$

where

$$\text{NONLIN} = \{v_j^{*\prime}T_j^{*\prime}\} - \{v_j^{*\prime}T_j^{*\prime}\}_c = \{v_j^{*\prime}T_j^{*\prime}\}' \quad \text{and}$$
$$\text{LIN} = \{v_j^{*\prime}T_c^*\} + \{v_c^*T_j^{*\prime}\}. \tag{3}$$

This decomposition highlights two terms that capture the interannual variability of $\{v^*T^*\}$: a term NONLIN that is quadratic in the wave anomaly represented by $v_j^{*\prime}$ and $T_j^{*\prime}$, and a term LIN that consists of terms that are linear in the wave anomaly. Locally (i.e., prior to zonal averaging), the LIN term is expected to dominate if the amplitude of the wave anomaly is small compared to the climatological wave. Under the zonal average, the sign and amplitude of the LIN term will depend in part on the degree of constructive or destructive interference between the climatological wave and the anomalous wave (Nishii et al. 2009; Garfinkel et al. 2010; Smith et al. 2010). The NONLIN term describes the component of the interannual variability of the total wave activity flux intrinsic to the wave anomalies themselves.

3. Results

a. Linear interference effects in interannual variability of wave activity

Before we use the $\{v^*T^*\}$ decomposition presented in section 2 to examine the relationship between snow cover and the NAM, we first examine the relative contributions of the LIN and NONLIN terms to the interannual variability of $\{v^*T^*\}$. We focus on the month of December, as this is the month when heat flux anomalies are most strongly correlated with October Eurasian snow cover anomalies (Cohen et al. 2007; Hardiman et al. 2008). The temporal variance of $\{v^*T^*\}$ can be decomposed as follows:

$$\begin{aligned}\mathrm{var}(\{v^*T^*\}) &= \mathrm{var}(\mathrm{LIN} + \mathrm{NONLIN}) \\ &= \mathrm{var}(\mathrm{LIN}) + \mathrm{var}(\mathrm{NONLIN}) \\ &\quad + 2\mathrm{cov}(\mathrm{LIN}, \mathrm{NONLIN}), \end{aligned} \tag{4}$$

where var(·) indicates the variance and cov(·) indicates the covariance. Using daily averaged v^* and T^* at 100 hPa, we first calculate $\{v^*T^*\}$, LIN, and NONLIN for each day of December (taking the meridional mean as described in section 2); then, we take the December mean of this result, which leads to an annual time series; and we then calculate the variance and covariance of the annual time series as measures of the interannual variability of the wave activity flux. We find var($\{v^*T^*\}$)= 12.05 m^2 K^2 s^{-2}, var(LIN) = 10.91 m^2 K^2 s^{-2}, var(NONLIN) = 4.13 m^2 K^2 s^{-2}, and 2cov(LIN, NONLIN) = −2.99 m^2 K^2 s^{-2}. When this calculation is repeated using December averaged v^* and T^* at 100 hPa as input, instead of daily data, we obtain 11.92, 10.99, 1.56, and −0.64 for these terms. The LIN term, therefore, describes the majority of the interannual variability in December $\{v^*T^*\}$. The total variance and the var(LIN) terms are similar whether monthly or daily data are used, while the variance contributions connected with the NONLIN terms are relatively large when daily data are used. This suggests that interannual variability in lower-stratospheric wave activity fluxes is dominated by variability in the low-frequency (quasi stationary) waves, while high-frequency waves dominate the NONLIN terms. Analogous behavior has been found in the simulated wave activity flux response to surface cooling (Smith et al. 2010). The LIN and NONLIN terms are slightly anticorrelated ($R = -0.22$) from year to year but the contribution of this to the total interannual variability is relatively small.

To quantify the relative importance of the synoptic time scale versus lower-frequency variability in the interannual variability of $\{v^*T^*\}$, we decompose $\{v^*T^*\}$ further into contributions from high- and low-frequency components. We perform a low-pass filter in the form of an 11-day running mean of v^* and T^* and approximate the high-pass-filtered v^* and T^* as

$$v^*_{\mathrm{high}} = v^* - v^*_{\mathrm{low}}, \quad T^*_{\mathrm{high}} = T^* - T^*_{\mathrm{low}}, \tag{5}$$

where $(\cdot)_{\mathrm{high}}$ is the high-frequency component of the eddies and $(\cdot)_{\mathrm{low}}$ is the low-frequency component of the eddies. Using (5), the variance of $\{v^*T^*\}$ then becomes

$$\begin{aligned}\mathrm{var}(\{v^*T^*\}) &= \mathrm{var}(\{v^*_{\mathrm{low}}T^*_{\mathrm{low}}\} + \{v^*_{\mathrm{high}}T^*_{\mathrm{low}}\} \\ &\quad + \{v^*_{\mathrm{low}}T^*_{\mathrm{high}}\} + \{v^*_{\mathrm{high}}T^*_{\mathrm{high}}\}) \end{aligned} \tag{6a}$$

$$\begin{aligned} &= \mathrm{var}(\{v^*_{\mathrm{low}}T^*_{\mathrm{low}}\}) + \mathrm{var}(\{v^*_{\mathrm{high}}T^*_{\mathrm{low}}\}) \\ &\quad + \mathrm{var}(\{v^*_{\mathrm{low}}T^*_{\mathrm{high}}\}) + \mathrm{var}(\{v^*_{\mathrm{high}}T^*_{\mathrm{high}}\}) \\ &\quad + \mathrm{COV}, \end{aligned} \tag{6b}$$

TABLE 1. Variance decomposition for December mean $\{v^*T^*\}$ at 100 hPa calculated using daily averaged NCEP–NCAR data from 1972 to 2008. Bold lettering indicates the total variance and the two dominant contributions to the variance.

Variance terms for December $\{v^*T^*\}$ at 100 hPa	Variance (m K s^{-1})^2
var(v^*T^*)	**12.05**
var($v^*_{\mathrm{low}}T^*_{\mathrm{low}}$)	**10.14**
var($v^*_{\mathrm{high}}T^*_{\mathrm{high}}$)	0.53
var($v^*_{\mathrm{low}}T^*_{\mathrm{high}}$)	0.12
var($v^*_{\mathrm{high}}T^*_{\mathrm{low}}$)	0.17
COV	1.09
var($\mathrm{LIN}_{\mathrm{low}}$)	**10.50**
var($\mathrm{NONLIN}_{\mathrm{low}}$)	2.45
2cov($\mathrm{LIN}_{\mathrm{low}}$, $\mathrm{NONLIN}_{\mathrm{low}}$)	−2.81

where COV represents the series of covariance terms in the expansion of Eq. (6a). From Table 1, we see that the variance of the time series of the December mean $\{v^*T^*\}$ at 100 hPa is dominated by the first term on the rhs of (6b), the low-frequency component of $\{v^*T^*\}$. The remaining variance terms are an order of magnitude smaller and the covariance terms contributing to COV are also relatively small (not shown). We can further decompose var($\{v^*_{\mathrm{low}}T^*_{\mathrm{low}}\}$) into its LIN and NONLIN components (Table 1), as in Eqs. (2) and (3), and find that the LIN term dominates. As expected, the interannual variability in the December meridional eddy heat flux for the high-pass eddies, which is represented by var($\{v^*_{\mathrm{high}}T^*_{\mathrm{high}}\}$), is dominated by the NONLIN term (not shown), and this represents the meridional eddy heat flux associated with high-pass transient eddies. However, var($\{v^*_{\mathrm{high}}T^*_{\mathrm{high}}\}$) represents a relatively small contribution (Table 1) to the 100-hPa December meridional eddy heat flux. This shows quantitatively that wintertime interannual variability in the vertical wave activity flux into the lower stratosphere is dominated by the terms that are linear in the low-frequency wave anomalies. The control of wintertime interannual variability in the wave activity flux by the low-frequency component of the flow provides a useful simplification in the dynamical understanding of NAM variability in the stratosphere and troposphere. Unfiltered daily data will be used for simplicity in the subsequent observational analysis, but these results justify the use of monthly data as input into the analysis of model output from the CMIP3 archive (section 3d).

We next examine the relative contributions of the LIN and NONLIN terms in transient NAM events that propagate from the stratosphere to the troposphere, which were first identified by Baldwin and Dunkerton (2001) and which are relevant to the discussion of the snow–NAM teleconnection in section 3b. Polvani and Waugh (2004) made the point that these events are initiated by wave activity flux anomalies propagating into

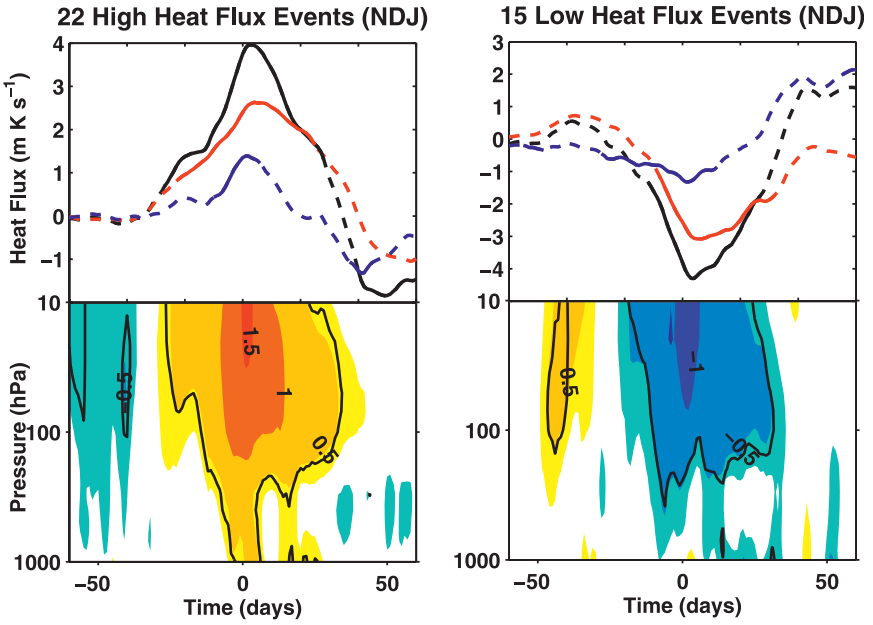

FIG. 1. (top) The time evolution of the November–January composite mean of the 40-day cumulative mean total meridional eddy heat flux ($\{v^*T^*\}$, black curve) anomalies at 100 hPa and the corresponding LIN (red curve) and NONLIN (blue curve) components for (left) 22 high and (right) 15 low anomalous $\{v^*T^*\}$ events. Solid sections of the heat flux curves indicate times when anomalies are different from zero at the level of 95% significance. (bottom) Composites of the time evolution of the standardized anomaly polar cap GPH corresponding to these anomalous $\{v^*T^*\}$ events as a function of pressure. The GPH contour interval is (0.25, 0.5, 1.0, 1.5); warm and cold shadings indicate positive and negative contours, respectively; and the black contour indicates pressures and times for which anomalies are different from zero at the level of 95% significance.

the stratosphere and construct time-lag composites of the NAM based on the occurrence of high or low wave activity flux anomaly conditions. Following a method similar to that used by Polvani and Waugh, we construct composites for the polar cap GPH anomalies based on anomalous 40-day cumulative average high and low wave activity flux events. Dynamically, the wave activity flux drives a tendency in the NAM on a multiple-week time scale; Polvani and Waugh use the cumulative mean heat flux instead of a centered running mean to produce a wave activity index that is temporally correlated with the NAM at zero lag. We focus on events from November–January (when we observe high correlations between October Eurasian snow cover and December heat fluxes) and construct composites on total heat flux anomalies, $\{v^*T^*\}'$, that exceed a threshold of 0.5 standard deviations and that are separated by at least 20 days (Fig. 1). The top row in Fig. 1 shows the composite daily time series of $\{v^*T^*\}'$ (black line), LIN (red line), and NONLIN (blue line) at 100 hPa for 22 high (left) and 15 low (right) total $\{v^*T^*\}'$ events. For these early to midwinter events, the anomalous wave activity flux events primarily consist of the LIN term; the NONLIN term is relatively small. The second row in Fig. 1 shows the composite of Z_{pcap} or NAM anomalies that correspond to the high and low $\{v^*T^*\}'$, as in Baldwin and Dunkerton (2001) and Polvani and Waugh (2004). Thus, our diagnostic confirms the result of Garfinkel et al. (2010) and demonstrates that linear interference is not only implicated in stratospheric NAM variability but also in NAM-related stratosphere–troposphere coupling.

b. *Linear interference in the snow–NAM link*

As has been previously shown (Cohen et al. 2007; Hardiman et al. 2008), October Eurasian snow cover is significantly and positively correlated with the vertical propagation of wave activity into the stratosphere in December and with stratosphere–troposphere NAM events in subsequent weeks. The basic snow–NAM connection is shown in Fig. 2a, which highlights the correlation between Z_{pcap} and OCTSNW for the years 1972–2009. For years with anomalously positive OCTSNW, a deep NAM anomaly builds from the troposphere to the stratosphere starting in mid-December and propagates back downward into the troposphere in February. We emphasize the

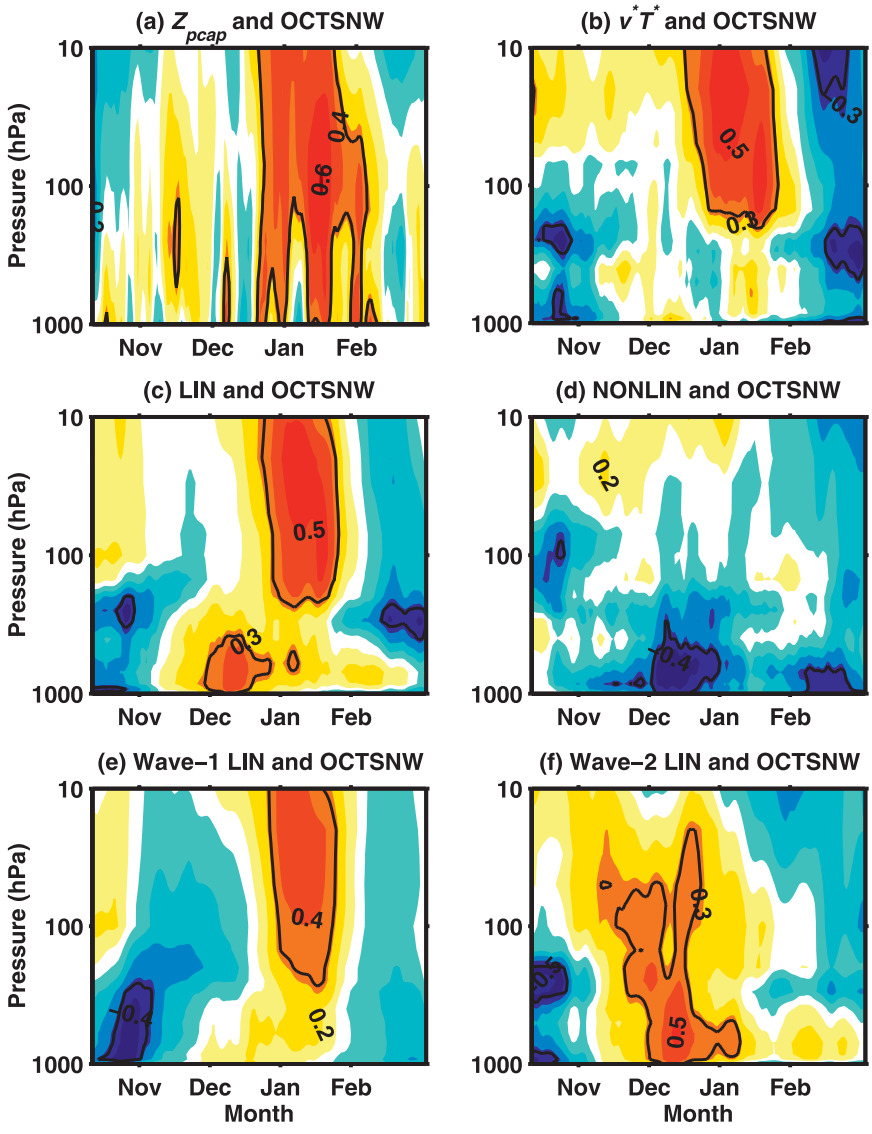

FIG. 2. Correlations of OCTSNW with daily (a) polar cap GPH, (b) the 40-day cumulative mean total meridional eddy heat flux averaged over 40°–80°N, (c) the LIN component of (b),(d) the NONLIN component of (b),(e) the wave-1 component of (c), and (f) the wave-2 component of (c). The time axis begins on 10 October. The contour interval is 0.1; warm and cold shadings are positive and negative contours, respectively; and the black contour indicates pressures and times for which correlations are different from 0 at the level of 95% significance.

remarkable persistence of this NAM signal, which lasts until February based on an October predictor.

The temporal evolution of geopotential coherent with OCTSNW resembles the climatological variability illustrated in the wave activity flux composites in Fig. 1, and so the main question is to determine how OCTSNW is consistently associated with positive wave activity flux events in winter. The connection to wave activity is shown in Fig. 2b, which shows the correlation of the 40-day cumulative mean meridional eddy heat flux with OCTSNW. There is a peak correlation in the lower stratosphere in January, corresponding to the peak warm period in Fig. 2a. Figures 2c,d show correlations analogous to Fig. 2b but for the LIN term and the NONLIN term, respectively. The correlation of the LIN term with OCTSNW is positive and significant in the troposphere in December and in the stratosphere in January and accounts for the significant positive correlation of $\{v^*T^*\}'$ with OCTSNW in the stratosphere. The NONLIN term is negatively correlated with OCTSNW in the troposphere in December and February and is not significantly correlated with OCTSNW in the stratosphere. The LIN and NONLIN terms

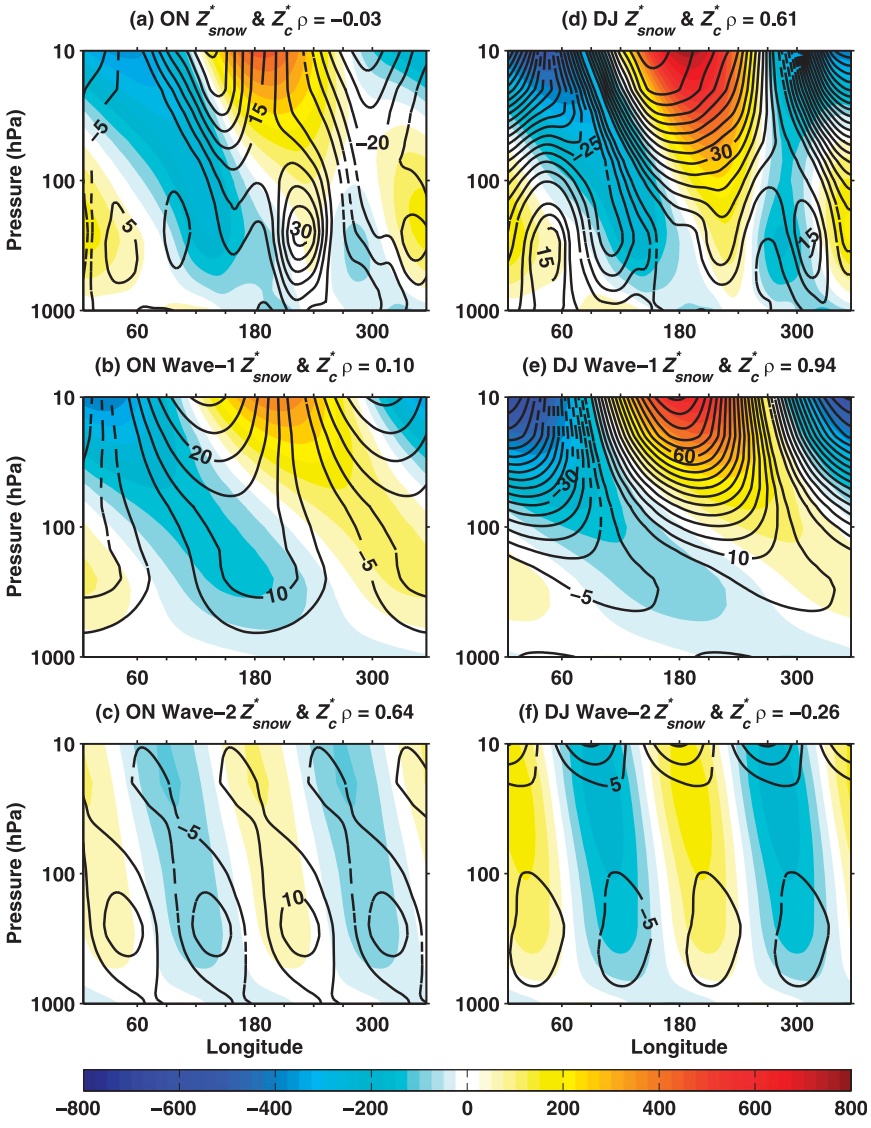

FIG. 3. Covariance of Z^* with OCTSNW (black contours) superimposed on Z^*_c (shading) at 60°N for (a)–(c) ON and (d)–(e) DJ. Also shown are (b),(e) the wave-1 and (c),(d) show wave-2 components of Z^*_{snow} and Z^*_c. Black solid and dashed contours show positive and negative values, respectively. The contour interval is 5 m.

associated with OCTSNW mostly cancel in the troposphere in December, resulting in no significant correlation between the total wave activity flux anomaly and OCTSNW. Figures 2e,f are similar to Fig. 2c except that they show the wave-1 and -2 components of LIN, respectively. The main features in Fig. 2c can be attributed to these two components of LIN: the positive correlations in the troposphere in December corresponding to the wave-2 LIN flux and those in the stratosphere in January corresponding to the wave-1 LIN flux. Figures 2c–f show that the cancellation between the LIN and NONLIN terms in the troposphere is primarily a cancellation between the wave-2 LIN flux and the NONLIN flux.

Since the LIN term explains most of the total wave activity flux correlation with the OCTSNW, the climatological stationary wave field and the wave field associated with the snow index must be constructively interfering prior to the peak wave activity flux in January. But our main interest is to ask why the LIN term is relatively small in the several weeks prior to this. A reduced LIN term might be associated with a relatively weak amplitude wave anomaly prior to December–January or with a linear interference effect, or a combination of the two. Hardiman et al. (2008) show that starting in October OCTSNW is significantly correlated with an upward-propagating wave train in the extratropics. Thus, the nature of the interference must be driving

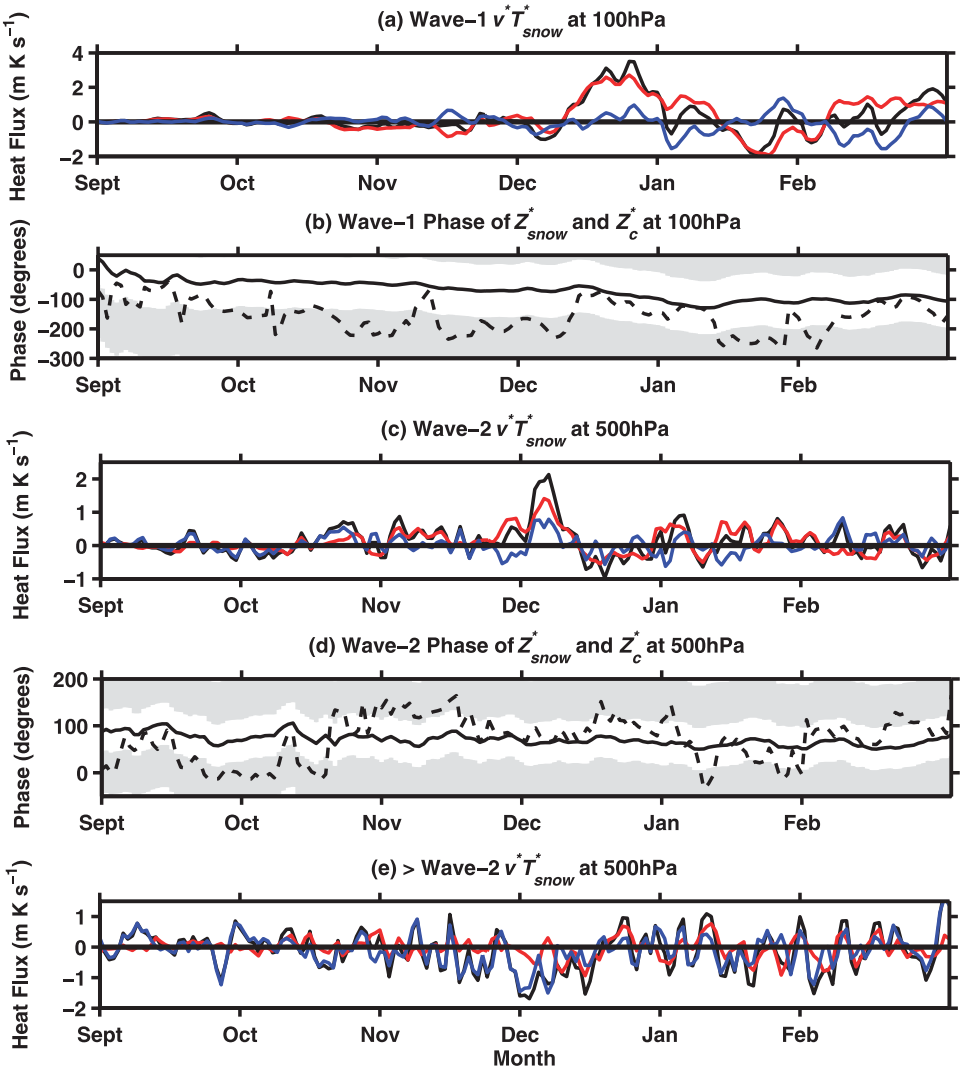

FIG. 4. Daily time series of (a) wave-1 40°–80°N-averaged zonal mean eddy meridional heat flux components at 100 hPa regressed on the snow index (total, black line; LIN_{snow}, red line; $NONLIN_{snow}$, blue line) and (b) the phase of the wave-1 component of Z^*_c for the 1972–2009 mean (solid line) and the phase of Z^*_{snow} (dashed line) at 60°N and 100 hPa. (c),(d) As in (a),(b), but for wave 2 at 500 hPa. (e) As in (d), but for all wavenumbers greater than wave 2. Gray shading in (a) and (c) indicates regions where Z^*_c and Z^*_{snow} are out of phase.

the lag between the snow anomalies and the wave activity fluxes. We confirm this conclusion by showing explicitly how the character of the interference evolves over time.

Figures 3a–f show the regressions of Z^* at 60°N with the OCTSNW, denoted Z^*_{snow}, and the wave-1 and -2 components superimposed on the climatological stationary waves, denoted Z^*_c, for 16 October–30 November (ON) and for 1 December–15 January (DJ) averages. The averaging periods are chosen to best illustrate the evolution of the meridional eddy heat flux correlations in Fig. 2. The wave anomaly associated with OCTSNW, Z^*_{snow}, undergoes a complicated transient evolution from ON to DJ, shifting eastward in both the troposphere and the stratosphere and at the same time amplifying in strength. The log-pressure weighted pattern correlations between Z^*_{snow} and the climatological stationary wave Z^*_c for ON are −0.03, 0.10, and 0.64 for all waves, wave 1, and wave 2, respectively, while the pattern correlations between Z^*_{snow} and Z^*_c for DJ are 0.61, 0.94, and −0.26 for all waves, wave 1, and wave 2, respectively. Thus, Z^*_{snow} and Z^*_c are in quadrature (neutrally in phase) in ON (Fig. 3a) and become strongly phase locked in DJ (Fig. 3d). The wave-1 component of Z^*_{snow} also increases in magnitude from ON to DJ (Figs. 3b,e) and becomes the wave component

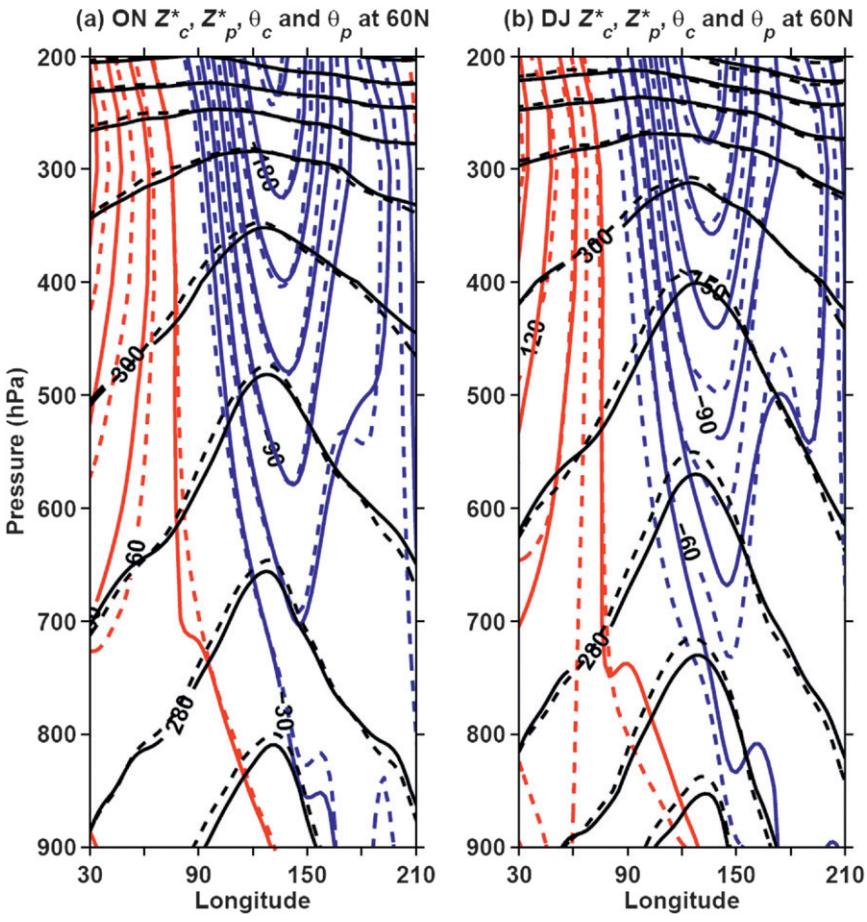

FIG. 5. As described in the text, the distribution of potential temperature (black contours) and wave GPH (red contours, positive; blue contours, negative) at 60°N associated with climatology (solid contours) and the climatology plus 2 times the regression on OCTSNW (dashed contours) for (a) ON and (b) DJ. Contour interval is 10 K for potential temperature and 30 m for wave GPH.

that best accounts for the correlation between LIN and OCTSNW in the stratosphere in January (Figs. 2b,c). Figure 3 also illustrates that the positive correlation between LIN and OCTSNW in the troposphere in December (Fig. 2c) is primarily associated with the positive phasing of the wave-2 components of Z^*_{snow} and Z^*_c (Fig. 3c). Since the amplitude of wave 2 is relatively small; however, the phasing of wave 1 determines the overall anomaly correlation between Z^*_{snow} and Z^*_c.

We now examine the transient evolution over the fall-to-winter season of the anomalous wave activity fluxes and the longitudinal phase structure of the climatological and anomalous waves separately for waves 1 and 2. Figure 4a shows the evolution of the stratospheric (100 hPa) wave-1 daily averaged wave activity flux regressed on OCTSNW, $v^*T^*_{\text{snow}}$, and its LIN and NONLIN components: LIN_{snow} and $\text{NONLIN}_{\text{snow}}$. We note that Fig. 4 plots daily $\{v^*T^*\}$ variations and not the 40-day cumulative mean variations, as in Figs. 1 and 2. The snow-related meridional eddy heat flux, $v^*T^*_{\text{snow}}$, starts increasing from near zero in about mid-December and achieves a broad peak throughout January. Overall, LIN_{snow} is the largest component during this time, corresponding to the peak in the 40-day cumulative wave-1 LIN in the stratosphere in early January in Fig. 2e. In Fig. 4b, the longitudinal phases of Z^*_{snow} with Z^*_c at 100 hPa are shown for wave 1; the gray shading indicates regions in which Z^*_{snow} and Z^*_c are out of phase. Although the phase of the wave anomaly is relatively noisy, Fig. 4b shows that the wave anomaly fluctuates in and out of phase with the climatology until December when it becomes phase locked with the climatological wave for about a month. This persistent phase locking allows for the development of sufficient upward wave activity to modify the stratospheric circulation.

In wave 2, the strongest snow-related LIN signals were found in the troposphere; thus, Figs. 4c,d are analogous

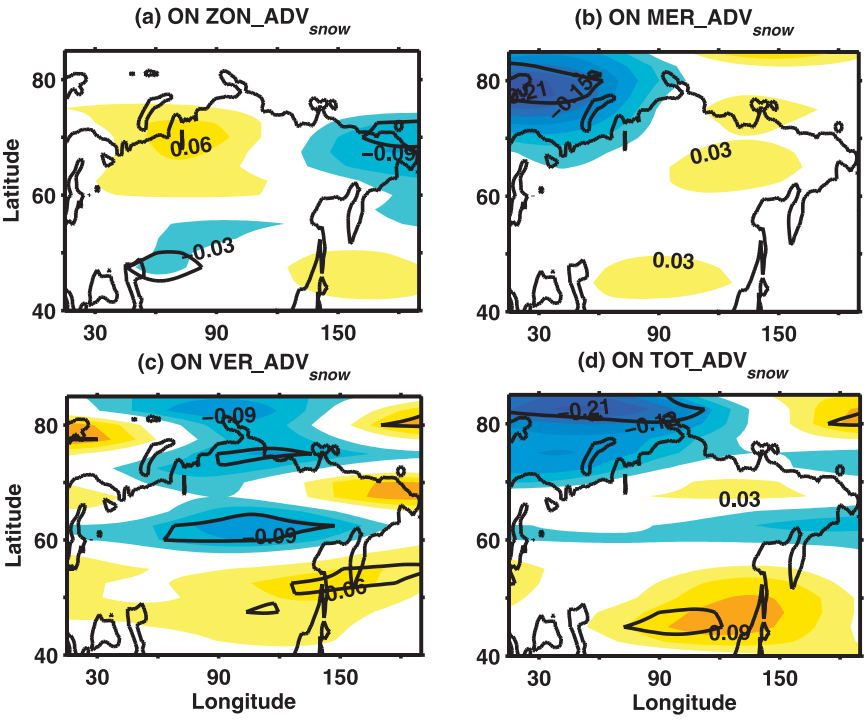

FIG. 6. The ON temperature advection: (a) ZON_ADV_{snow}, (b) MER_ADV_{snow}, (c) $VERT\_ADV_{snow}$, and (d) TOT_ADV_{snow} vertically integrated from 925 to 700 hPa and filtered to retain wavenumbers 1–3. The contour interval is 0.03 K day^{-1}; warm and cold shadings show positive and negative contours, respectively; and the black contour indicates regions for which correlations are different from zero at the level of 95% significance.

to Figs. 4a,b but for the 500-hPa wave-2 meridional eddy heat flux and longitudinal phase. Again, LIN_{snow} is dominant although not as much as it was for wave 1 in the stratosphere. It begins to increase in late November, corresponding to the tropospheric peak shown in Fig. 2f in mid-December. Figure 4d shows that its increase is largely reflected in the phasing between the anomalous and climatological waves. As in Fig. 4b, we see a period of about 3 weeks where the waves are phase locked. Finally, Fig. 4e shows the 500-hPa meridional eddy heat fluxes corresponding to all wave components greater than wave 2. Unlike Figs. 4a,c, Fig. 4e shows that contributions to tropospheric heat fluxes at smaller scales are dominated by $NONLIN_{snow}$. Specifically, in early December a negative peak in $NONLIN_{snow}$ and, thus, $v^*T^*_{snow}$ is observed, corresponding to the negative correlations in the troposphere in mid-December shown in Fig. 2d.

In summary, the lag between the peak in snow cover anomalies in October and the peak in the corresponding wave activity flux into the stratosphere (Fig. 2b) can be partially explained by the lack of persistent constructive interference in the dominant stratospheric wave component, wave 1, until December. Although there is a seasonal westward shift of Z^*_c, the phasing is primarily determined by the zonal propagation of Z^*_{snow} (Figs. 4b and 4d). What causes Z^*_{snow} to shift zonally remains to be explained.

We have pursued two additional lines of dynamical analysis to attempt to explain the eastward shift and amplification of Z^*_{snow} from October to December. First, we present diagnostics related to the evolution of the form stress anomaly associated with Eurasian snow cover extent variability. In their modeling study, Fletcher et al. (2009) describe how tropospheric isentropes dome up as a result of the snow-induced cooling and argue that this induces an upstream high–downstream low circulation pattern, via potential vorticity conservation, and a corresponding positive form stress anomaly consistent with the anomalous upward propagation of wave activity. Qualitative observational support for this viewpoint is shown in Fig. 5, which shows the climatological distribution of potential temperature (in solid black contours), the climatological wave GPH (solid colored contours), the total potential temperature coherent with OCTSNW (climatology plus 2 times the regression on OCTSNW, denoted with a subscript p, dashed black), and the total wave GPH coherent with OCTSNW (climatology plus 2 times the regression on OCTSNW, denoted with a subscript p, dashed color). The plots are repeated for the same time periods as in Fig. 3.

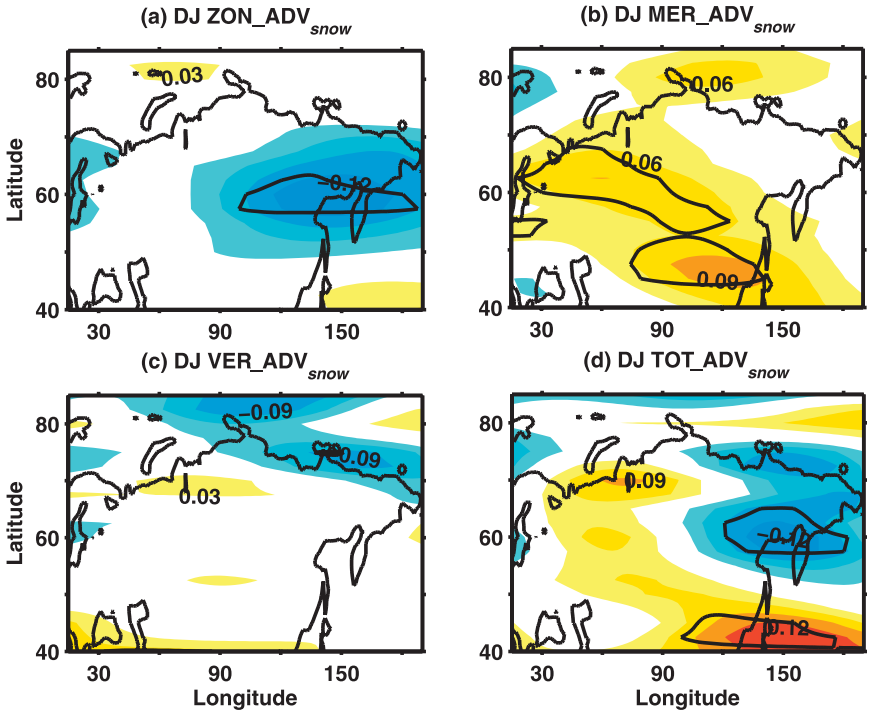

FIG. 7. As in Fig. 6, but for the DJ temperature advection.

Figure 5 shows a persistent doming up of potential temperature surfaces coherent with OCTSNW, and a circulation anomaly corresponding to the intensification of the climatological high to the west and the climatological low to the east of the isentropic peak near 130°E from ON to DJ. In isobaric coordinates, one may write the meridional eddy heat flux anomaly as a form stress anomaly, $\{v^*T^*\}' \sim \{\tilde{p}^*\partial Z^*/\partial x\}' = \{-Z^*\partial\tilde{p}^*/\partial x\}'$, where $\tilde{p}^*$ denotes the perturbation pressure of the isentropic surface θ^* and the braces denote the zonal mean. Figure 5 illustrates the two components of the form stress that contribute to LIN. The first component involves the steepening or shallowing of perturbation isentropes relative to the climatology and the second corresponds to the steepening or shallowing of the perturbation geopotential gradients relative to the climatology. A more detailed analysis (not shown) reveals that in the zonal mean both components are generally positive (corresponding to an upward LIN wave activity flux anomaly) and that the second component dominates. Consistent with Figs. 3 and 4, the geopotential wave anomaly shifts to the east and intensifies, but there is no obvious eastward shift of the potential temperature distribution. The latter implies that the shift in the longitudinal phase of the Rossby wave response to snow forcing is not associated with a shift in the location of the forcing itself.

Second, we present diagnostics related to dynamical heating in the lower troposphere. Using daily data, we find (not shown) that advective heating in the lower troposphere is dominated by linear terms. We show in Figs. 6 and 7 that these linear terms undergo a striking change as the season evolves. Figure 6 shows the ON zonal, meridional, vertical, and total temperature advection integrated from 925 to 700 hPa and filtered to retain wavenumbers 1–3 regressed on OCTSNW; we call the corresponding terms $\text{ZON\_ADV}_{\text{snow}}$, $\text{MER\_ADV}_{\text{snow}}$, $\text{VERT\_ADV}_{\text{snow}}$, and $\text{TOT\_ADV}_{\text{snow}}$. In ON, the vertical advection term $\text{VERT\_ADV}_{\text{snow}}$ over Eurasia is negative and statistically significant. This cooling is partially canceled by weak warming from $\text{ZON\_ADV}_{\text{snow}}$ and $\text{MER\_ADV}_{\text{snow}}$, so that $\text{TOT\_ADV}_{\text{snow}}$ is only weakly negative and statistically insignificant over the continent. There is also a region of negative $\text{MER\_ADV}_{\text{snow}}$ north of Scandinavia, consistent with destructive interference near the western periphery of the Siberian high in ON, weakening poleward temperature advection (Panagiotopoulos et al. 2005). In DJ (Fig. 7), the horizontal terms $\text{ZON\_ADV}_{\text{snow}}$ and $\text{MER\_ADV}_{\text{snow}}$ are dominant and statistically significant, and correspond to a relatively strong cooling on the eastern coast of Eurasia near 60°N. A warming center associated with vertical advection in ON and meridional advection in DJ is present near 40°N, 150°E. Thus, the advective heating associated with Eurasian snow cover changes from being dominated by vertical advection to horizontal advection as the season progresses. There is also a suggestion of an eastward shift and intensification

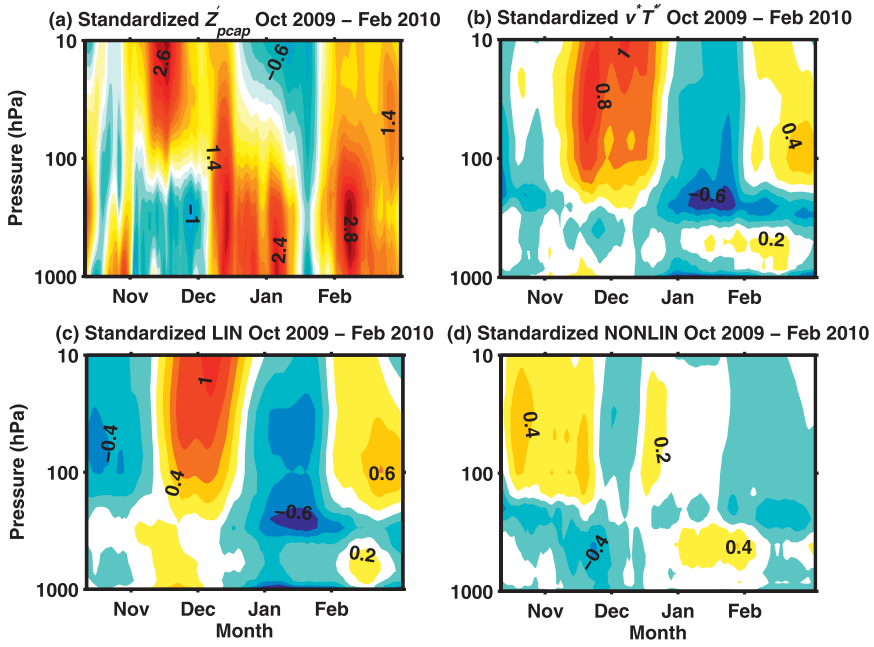

FIG. 8. Daily standardized (a) Z'_{pcap} and the 40-day averaged(b) 40°–80°N $\{v^*T^*\}'$, (c) the LIN component of (b), and (d) the NONLIN component of (b). The X axis begins on 10 Oct 2009 and ends on 29 Feb 2010. The contour interval is 0.2 standard deviation units and warm and cold shadings show positive and negative contours, respectively.

of this heating. We have found that classical analyses of stationary wave dynamics (e.g., Hoskins and Karoly 1981) do not explain this behavior and are currently investigating its dynamics in simplified GCMs of the kind used in Smith et al. (2010).

c. *Case study: Winter 2009/10*

Cohen et al. (2010, hereafter C10) has argued that the strong negative NAM events of the 2009/10 winter season reflected snow-forced NAM dynamics; here, we investigate this season from the perspective of linear interference diagnostics. Although Eurasian snow cover extent was initially below normal in early October 2009, by the end of the month it was the greatest it has been since its maximum observed value in 1976. C10 connect this anomalous snow cover extent to the subsequent negative NAM events in November–December and February and demonstrate that a statistical forecast model including October Eurasian snow cover extent captured the spatial pattern of anomalously cold 2009/10 winter European surface temperatures. We present a complementary analysis demonstrating that the two negative NAM events highlighted in C10 were preceded by anomalous upward LIN wave activity fluxes resulting from constructive interference between the anomalous wave and the background climatological stationary wave.

Figure 8a shows the standardized polar cap averaged GPH anomaly Z'_{pcap} from mid-October to the end of February, analogous to Fig. 1a in C10. The two negative NAM events are clearly visible in November–December and early February, the second being a major sudden stratospheric warming. Figures 8b–d show the standardized 40-day cumulative $\{v^*T^*\}'$, LIN, and NONLIN over the same time period (LIN and NONLIN are standardized by the standard deviation of $\{v^*T^*\}$). The two negative NAM events are associated with positive $\{v^*T^*\}'$ (see also C10's Fig. 1b). The majority of $\{v^*T^*\}'$ is associated with LIN (Fig. 8c). The contribution from NONLIN is relatively small (Fig. 8d). Based on the analysis in sections 3a and 3b, this result suggests that $\{v^*T^*\}'$ is associated with an anomalous wave that constructively interferes with the background climatological wave prior to the two negative NAM events. Figure 9a shows the anomalous wave, $Z^{*\prime}$ superimposed on Z_c^* at 60°N for November, when the LIN wave activity fluxes are positive. The pattern correlation between these two wave fields is 0.43. The wave-1 components of the waves are highly correlated at 0.66 (Fig. 9b). Contrastingly, in December when the 40-day cumulative LIN switches from positive to negative (Fig. 8c), the pattern correlation between $Z^{*\prime}$ and Z_c^* is negative (−0.36; Fig. 9c). Analysis of the time series of the phase of wave-1 $Z^{*\prime}$ and Z_c^* in the stratosphere (not shown)

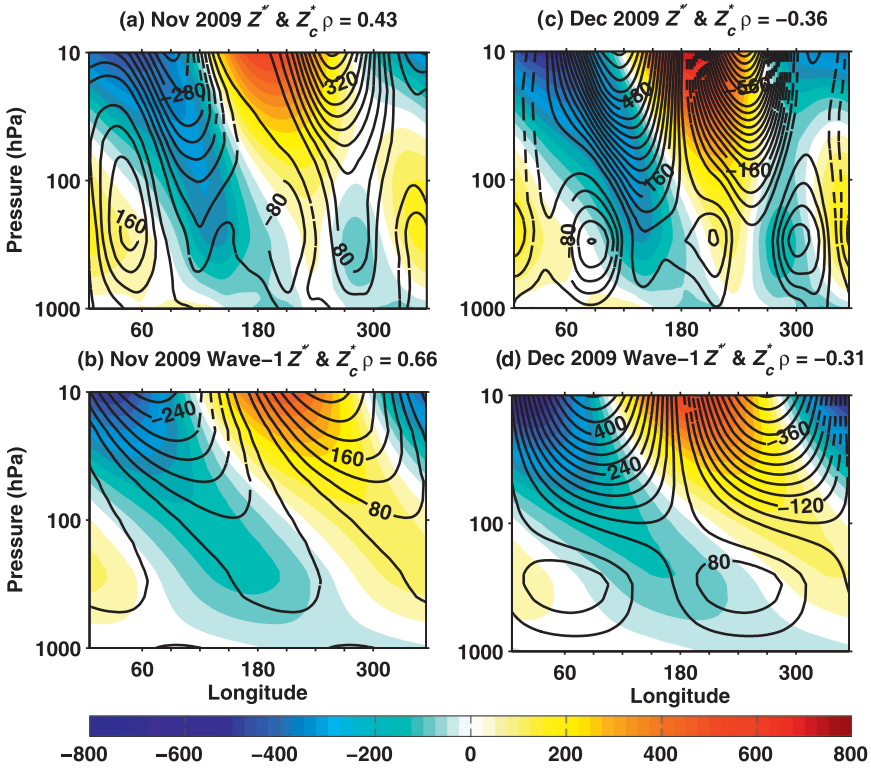

FIG. 9. The $Z^{*\prime}$ (black contours) superimposed on Z_c^* (shading) at 60°N for (a),(b) November and (c),(d) December 2009. Also shown are the wave-1 components (b) $Z^{*\prime}$ and (d) Z_c^*. Black solid and dashed contours show positive and negative values, respectively. The contour interval is 40 m.

indicates that the waves become phase locked approximately 2–3 weeks prior to the appearance of the negative NAM in the stratosphere. For the first negative NAM event, this timing is consistent with October Eurasian snow cover anomalies influencing the anomalous wave but the analysis presented here does not reflect the snow–NAM connection directly. In addition, the relatively persistent phase locking suggests that linear interference diagnostics may improve the predictability of other NAM events.

In summary, the dynamical evolution of the NAM in the 2009/10 winter season is dominated by linear contributions to the wave activity, and the two negative NAM events of that season correspond to two constructive linear interference events. These results complement the analysis of C10 and highlight the potential utility of linear interference diagnostics for seasonal forecasting.

d. *Linear interference and the snow–NAM link in CMIP3 models*

Table 2 shows the contributions to the interannual variance of the terms in the decomposition in Eq. (4) for the $\{v^*T^*\}$ time series at 100 hPa for the twentieth century simulations of the CMIP3 models. The interannual variance of $\{v^*T^*\}$ is generally weak in the models, so the contribution of the variance in LIN and in NONLIN and the covariance between the two are divided by the variance in the total in the third, fourth, and fifth columns of Table 2. In the models, the linear interference effect is dominant as in NCEP, but the contributions from var(NONLIN) and 2cov(LIN, NONLIN) are generally larger than in NCEP and less well separated from the LIN contribution. This is due in part to the fact that the stationary waves are typically too weak in the CMIP3 models relative to observations. Table 3 shows the amplitude of the wave-1 component of the wintertime (December–February, DJF) Z_c^* at 60°N and 50 hPa for NCEP and for each model. All models except one have weaker amplitudes than NCEP. We find that the wave-1 amplitude is weakly positively correlated with var($\{v^*T^*\}$) across the models ($R^2 = 0.26$) and with the quantity var(LIN)/var(NONLIN) ($R^2 = 0.25$). This suggests that larger simulated wave-1 amplitudes are associated with larger interannual variability in wave activity fluxes and stronger linear interference. Conversely, the bias towards weak stationary wave amplitudes in the CMIP3 models implies that wave activity fluxes dominated by linear interference effects might not be well estimated in these models.

TABLE 2. Variance decomposition for December mean $\{v^*T^*\}$ at 100 hPa calculated using monthly averaged CMIP3 model archive data for twentieth-century runs.

Model	var($\{v^*T^*\}$)	Fraction of var($\{v^*T^*\}$) from var(LIN)	Fraction of var($\{v^*T^*\}$) from var(NONLIN)	Fraction of var($\{v^*T^*\}$) from 2cov(LIN, NONLIN)
NCEP	11.92	0.92	0.13	−0.05
cccma_cgcm3_1	7.70	1.28	0.22	−0.5
cccma_cgcm3_1_t63	6.48	1.26	0.21	−0.47
cnrm_cm3	4.25	0.95	0.17	−0.12
csiro_mk3_0	2.02	0.84	0.40	−0.24
gfdl_cm2_0	5.88	1.08	0.17	−0.25
gfdl_cm2_1	6.66	1.06	0.19	−0.24
giss_model_e_r	3.55	1.04	0.10	−0.14
iap_fgoals1_0_g	8.59	0.96	0.19	−0.14
inmcm3_0	9.84	1.08	0.17	−0.26
ipsl_cm4	6.74	0.96	0.21	−0.18
miroc3_2_medres	2.64	0.92	0.24	−0.17
mpi_echam5	8.87	0.98	0.20	−0.18
mri_cgcm2_3_2a	9.82	0.89	0.13	−0.02
ncar_ccsm3_0	13.23	0.89	0.35	−0.24
ukmo_hadgem1	8.82	0.82	0.19	−0.01

Hardiman et al. (2008) demonstrated that comprehensive GCMs, including the CMIP3 models, fail to reproduce the negative correlation between October Eurasian snow cover and the wintertime NAM. They attributed this behavior primarily to the fact that the wave anomaly associated with the snow cover in the GCMs is unrealistically small scale and cannot therefore effectively propagate into the stratosphere. To supplement the Hardiman et al. analysis, we investigate the role of linear interference in the snow–NAM relationship in GCMs. We conduct calculations analogous to those presented in section 3b; however, we are restricted to using monthly averaged data available from the simulation archive. Figure 10 shows a scatterplot of the correlation between December $\{v^*T^*\}'$ at 100 hPa and the October Eurasian snow index [as in Hardiman et al. (2008), but with a slightly different set of models represented] versus the correlation between 40° and 80°N zonal mean LIN at 100 hPa and the October Eurasian snow index for each model (OCTSNW-M). As in the observations, we see a positive linear relationship between these two quantities, consistent with the LIN terms dominating the wave activity flux in the simulations. However, Fig. 10 illustrates that the majority of the models produce negative correlations between $\{v^*T^*\}$ and OCTSNW-M and that this is mostly explained ($R^2 = 0.63$) by the negative correlation between the LIN term and OCTSNW-M. In addition, there is a significant amount of spread between the models and no model captures the strong correlations illustrated in Fig. 2 between LIN and OCTSNW in the observations: if the observational data were plotted in Fig. 10, they would be located at (0.36, 0.50).

We have investigated whether other factors may also explain the spread along the x axis in Fig. 10. A plot analogous to Fig. 10 but substituting the NONLIN term for the LIN term shows no significant relationship (figure not shown), suggesting that snow-related driving of the NONLIN term is not an important factor in explaining the spread. In addition, there is no relationship between the magnitude of interannual October Eurasian snow cover variability (Hardiman et al. 2008) or the mean October Eurasian snow cover and a model's ability to simulate the observed snow–NAM relationship.

Closer examination of two individual models reveals how inconsistently the linear interference effect can be

TABLE 3. Amplitude of the wave-1 component of December–February Z_c^* at 60°N and 50 hPa for NCEP–NCAR (1972–2009) and the CMIP3 model archive data for twentieth-century runs.

Model	Amplitude of wave-1 Z_c^* at 60°N and 50 hPa (m)
NCEP	229
cccma_cgcm3_1	224
cccma_cgcm3_1_t63	172
cnrm_cm3	220
csiro_mk3_0	56
gfdl_cm2_0	137
gfdl_cm2_1	183
giss_model_e_r	207
iap_fgoals1_0_g	150
inmcm3_0	219
ipsl_cm4	81
miroc3_2_medres	114
mpi_echam5	162
mri_cgcm2_3_2a	319
ncar_ccsm3_0	194
ukmo_hadgem1	208

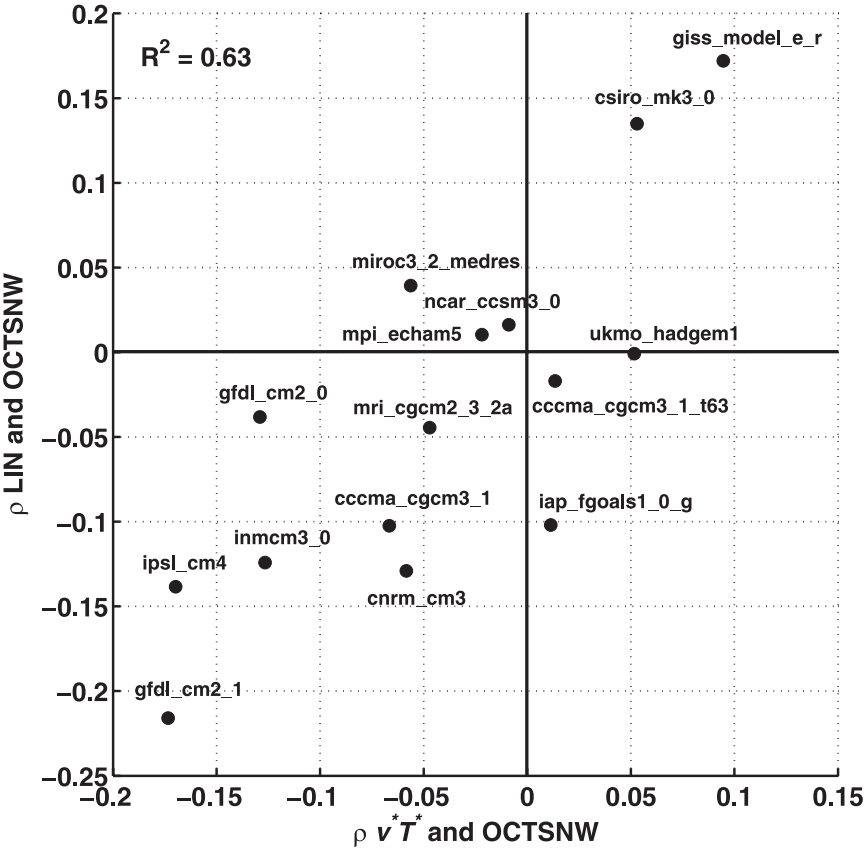

FIG. 10. Scatterplot of the correlation between December $\{v^*T^*\}$ and OCTSNW-M and the correlation between December LIN and OCTSNW-M for each model.

represented in different models. Figure 11 shows plots similar to those in Fig. 3 but for the Goddard Institute for Space Studies (GISS) model (Figs. 11a,c) and the Geophysical Fluid Dynamics Laboratory Climate Model version 2.1 (GFDL CM2.1; see Figs. 11b,d), respectively. The GISS model produces a positive correlation between December wave activity fluxes and OCTSNW-M while GFDL CM2.1 produces a negative correlation (see Fig. 10). The pattern correlations for the ON and DJ means for the GISS model are 0.15 and 0.03 (Figs. 11a,c), respectively, while for GFDL CM2.1 they are -0.42 and -0.26 (Figs. 11b,d). Although LIN regressed on OCTSNW, LIN_{snow}, is by far the dominant component in $v^*T^*_{\text{snow}}$ for both of these models, the pattern correlations in Fig. 11 are somewhat weak. Weak phasing combined with the weaker amplitude of both Z^*_{snow} and Z^*_c in the models leads to a relatively weak LIN_{snow} compared with the observations. As illustrated in section 3c, many factors might drive this pattern of nonrobust behavior, including variations in how surface cooling affects stratification, in the relative roles of horizontal and vertical advection, and in the stationary wave simulation; no single factor stands out in explaining the spread at this point.

4. Conclusions

In this study we illustrate how linear interference plays a dominant role in describing the wintertime interannual variability of the vertical component of the wave activity flux into the stratosphere, represented by the zonal mean extratropical meridional eddy heat fluxes $\{v^*T^*\}$. This is accomplished by decomposing $\{v^*T^*\}$ into a linear interference component, LIN, and a nonlinear component, NONLIN. We demonstrate that the variability of the low-frequency component of LIN accounts for the majority of the wintertime interannual $\{v^*T^*\}$ variance in the upper troposphere while the variance of NONLIN arises primarily from high-frequency eddies (Table 1). In the middle and lower troposphere, NONLIN variability increases as high-frequency eddy variability increases. Extending the work of Polvani and Waugh (2004) and Garfinkel et al. (2010), we show that anomalous wintertime wave activity flux events associated with zonal mean high-latitude stratospheric variability are dominated by contributions that are linear in the amplitude of the wave anomalies and that correspond to events in which wave anomalies constructively or destructively interfere with

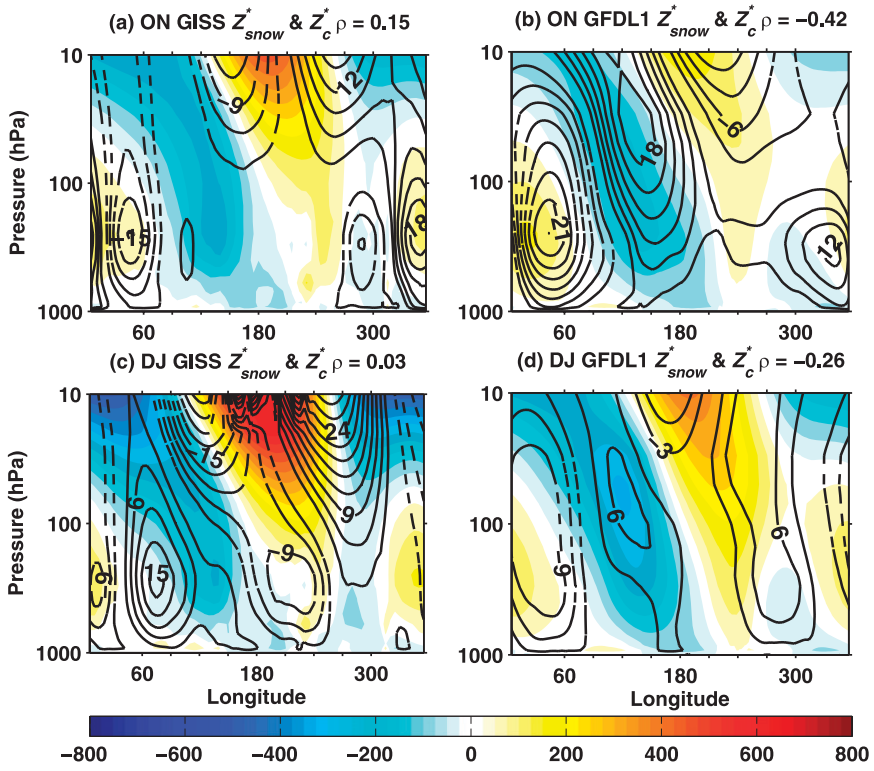

FIG. 11. October–November mean Z^*_{snow} (black contours) superimposed on the Z^*_c (shading) at 60°N for the (a) GISS and (b) GFDL CM2.1 models. (c),(d) As in (a),(b), but for December–January. The contour interval is 3 m.

the climatological wave field. Analysis of linear interference outside the winter season is ongoing.

Our main novel contribution has been to examine the relationship between October Eurasian snow cover anomalies and the NAM within the context of linear interference. The lag between October Eurasian snow cover index (OCTSNW) and December–January wave activity flux is shown to be related to the lack of favorable linear interference conditions prior to December–January. Several studies have identified a regional relationship between autumn Eurasian snow cover and Eurasian/Pacific sector circulation patterns. For example, Orsolini and Kvamsto (2009) and Wu et al. (2011) highlight a connection to a Pacific–North American circulation pattern, but Garfinkel et al. (2010) highlight a connection to an eastern European high and northwestern Pacific low pattern. Although there is some inconsistency concerning which specific wave patterns are linked to snow, our conclusion is that in December the planetary-scale wave train associated with OCTSNW shifts into phase with the background wave, and the vertical wave activity, represented by the meridional eddy heat flux, is amplified (Fig. 4). Accompanying the shift in the wave train associated with the OCTSNW changes are an intensification of the source of anomalous form stress from the troposphere and a shift in advective heating in the lower troposphere from vertical advection dominated to horizontal advection dominated. We also present a case study showing that the two strong negative NAM events of the 2009/10 winter (Cohen et al. 2010) were preceded by upward LIN wave activity fluxes into the stratosphere. We show that the anomalous wave phase locks with the background climatological wave 2–3 weeks preceding the NAM events, leading to strong 40-day cumulative LIN wave activity fluxes.

Finally, we revisit the issue of the inability of current climate models to capture the snow cover–NAM connection (Hardiman et al. 2008). Most models show a connection of opposite sign to the observed between October Eurasian snow extent and December wave activity and this negative correlation is shown to be a linear interference effect: in the models, years with greater October Eurasian snow extent typically lead to a weakening of the wintertime wave pattern. Since CMIP3 models generally reproduce the phase of the climatological background waves fairly well (Brandefelt and Kornich 2008), these results suggest that the wave anomaly in the models associated with the snow cover is not evolving in the same manner as in the observations.

Although this study demonstrates that linear interference can affect the sign and timing of the relationship

between October Eurasian snow cover anomalies, $\{v^*T^*\}$ and the NAM, a detailed analysis of what causes the shift in the phase of the wave train associated with a relatively stationary surface forcing, such as snow cover, remains to be done. This work provides pointers to follow-on research required to understand the nuanced and sensitive relationships operating in this aspect of extratropical variability. For example, Fig. 5 suggests that the diabatic heating associated with snow remains relatively stationary, but that the wave anomaly associated with the snow undergoes a much more complicated transient evolution. This implies that it would be useful to investigate the linear transient response to stationary surface cooling. In addition, further investigation of the transient evolution of climatological LIN events may provide insights into the snow–NAM problem. Current work along these lines is ongoing.

Acknowledgments. KLS and PJK acknowledge the support of the Natural Sciences and Engineering Research Council of Canada, the Canadian Foundation for Climate and Atmospheric Sciences (Grant 506), and the Canadian International Polar Year Cryosphere Network. JC is supported by National Science Foundation Grants ARC-0909459 and ARC-0909457 and NOAA Grant NA10OAR4310163.

REFERENCES

Allen, R. J., and C. S. Zender, 2010: Effects of continental-scale snow albedo anomalies on the wintertime Arctic oscillation. *J. Geophys. Res.,* **115,** D23105, doi:10.1029/2010JD014490.

Baldwin, M. P., and T. P. Dunkerton, 2001: Stratospheric harbingers of anomalous weather regimes. *Science,* **294,** 581–584.

——, and D. W. J. Thompson, 2009: A critical comparison of stratosphere–troposphere coupling indices. *Quart. J. Roy. Meteor. Soc.,* **135,** 1661–1672.

Brandefelt, J., and H. Kornich, 2008: Northern Hemisphere stationary waves in future climate projections. *J. Climate,* **21,** 6341–6353.

Brown, R. D., and P. Mote, 2009: The response of Northern Hemisphere snow cover to a changing climate. *J. Climate,* **22,** 2124–2145.

Cohen, J., and D. Rind, 1991: The effect of snow cover on the climate. *J. Climate,* **4,** 689–706.

——, and D. Entekhabi, 1999: Eurasian snow cover variability and Northern Hemisphere climate predictability. *Geophys. Res. Lett.,* **26,** 345–348.

——, and C. Fletcher, 2007: Northern Hemisphere winter surface temperature predictions based on land–atmosphere fall anomalies. *J. Climate,* **20,** 4118–4132.

——, D. Salstein, and K. Saito, 2002: A dynamical framework to understand and predict the major Northern Hemisphere mode. *Geophys. Res. Lett.,* **29,** 1412, doi:10.1029/2001GL014117.

——, M. Barlow, P. Kushner, and K. Saito, 2007: Stratosphere–troposphere coupling and links with Eurasian land-surface variability. *J. Climate,* **20,** 5335–5343.

——, J. Foster, M. Barlow, K. Saito, and J. Jones, 2010: Winter 2009–2010: A case study of an extreme Arctic Oscillation event. *Geophys. Res. Lett.,* **37,** L17707, doi:10.1029/2010GL044256.

Fletcher, C. G., and P. J. Kushner, 2011: The role of linear interference in the annular mode response to tropical SST forcing. *J. Climate,* **24,** 778–794.

——, ——, and J. Cohen, 2007: Stratospheric control of the extratropical circulation response to surface forcing. *Geophys. Res. Lett.,* **34,** L21802, doi:10.1029/2007GL031626.

——, S. C. Hardiman, P. J. Kushner, and J. Cohen, 2009: The dynamical response to snow cover perturbations in a large ensemble of atmospheric GCM integrations. *J. Climate,* **22,** 1208–1222.

Foster, J., M. Owe, and A. Rango, 1983: Snow cover and temperature relationships in North America and Eurasia. *J. Climate Appl. Meteor.,* **22,** 460–469.

Garfinkel, C. I., D. L. Hartmann, and F. Sassi, 2010: Tropospheric precursors of anomalous Northern Hemisphere stratospheric polar vortices. *J. Climate,* **23,** 3282–3299.

Gong, G., D. Entekhabi, and J. Cohen, 2002: A large-ensemble model study of the wintertime AO/NAO and the role of interannual snow perturbations. *J. Climate,* **15,** 3488–3499.

——, ——, and ——, 2003: Modeled Northern Hemisphere winter climate response to realistic Siberian snow anomalies. *J. Climate,* **16,** 3917–3931.

Groisman, P. Ya., T. R. Karl, and R. W. Knight, 1994: Changes of snow cover, temperature, and radiative heat balance. *J. Climate,* **7,** 1633–1656.

Hardiman, S. C., P. J. Kushner, and J. Cohen, 2008: Investigating the effect of fall Eurasian snow cover on winter climate in general circulation models. *J. Geophys. Res.,* **113,** D21123, doi:10.1029/2008JD010623.

Henderson, G. R., and D. J. Leathers, 2009: European snow cover extent variability and associations with atmospheric forcings. *Int. J. Climatol.,* **30,** 1440–1451, doi:10.1002/joc.1990.

Hoskins, B. J., and D. J. Karoly, 1981: The steady linear response of a spherical atmosphere to thermal and orographic forcing. *J. Atmos. Sci.,* **38,** 1179–1196.

Ineson, S., and A. A. Scaife, 2009: The role of the stratosphere in the European response to El Niño. *Nat. Geosci.,* **2,** 32–36, doi:10.1038/NGEO381.

Kalnay, E., and Coauthors, 1996: The NCEP/NCAR 40-Year Reanalysis Project. *Bull. Amer. Meteor. Soc.,* **77,** 437–471.

Kolstad, E. W., and A. J. Charlton-Perez, 2010: Observed and simulated precursors of stratospheric polar vortex anomalies in the Northern Hemisphere. *Climate Dyn.,* **37,** 1443–1456, doi:10.1007/s00382-010-0919-7.

Martius, O., L. M. Polvani, and H. C. Davies, 2009: Blocking precursors to stratospheric sudden warming events. *Geophys. Res. Lett.,* **36,** L14806, doi:10.1029/2009GL038776.

Mote, T., 2008: On the role of snow cover in depressing air temperature. *J. Appl. Meteor. Climatol.,* **47,** 2008–2022.

Newman, P. A., E. R. Nash, and J. E. Rosenfield, 2001: What controls the temperature of the Arctic stratosphere during the spring?. *J. Geophys. Res.,* **106** (D17), 19 999–20 010.

Nishii, K., H. Nakamura, and T. Miyasaka, 2009: Modulations in the planetary wave field induced by upward-propagating Rossby wave packets prior to stratospheric sudden warming events: A case study. *Quart. J. Roy. Meteor. Soc.,* **135,** 39–52.

——, ——, and Y. J. Orsolini, 2010: Cooling of the wintertime Arctic stratosphere induced by the western Pacific teleconnection pattern. *Geophys. Res. Lett.,* **37,** L13805, doi:10.1029/2010GL043551.

Orsolini, Y. J., and N. G. Kvamsto, 2009: Role of Eurasian snow cover in wintertime circulation: Decadal simulations forced with satellite observations. *J. Geophys. Res.,* **114,** D19108, doi:10.1029/2009jD012253.

Panagiotopoulos, F., M. Shahgedanova, A. Hannachi, and D. B. Stephenson, 2005: Observed trends and teleconnections of the Siberian high: A recently declining center of action. *J. Climate,* **18,** 1411–1422.

Polvani, L. M., and D. W. Waugh, 2004: Upward wave activity flux as precursor to extreme stratospheric events and subsequent anomalous surface weather regimes. *J. Climate,* **17,** 3548–3554.

Robinson, D. A., K. F. Dewey, and R. R. Heim, 1993: Global snow cover monitoring: An update. *Bull. Amer. Meteor. Soc.,* **74,** 1689–1696.

Smith, K. L., C. G. Fletcher, and P. J. Kushner, 2010: The role of linear interference in the annular mode response to extratropical surface forcing. *J. Climate,* **23,** 6036–6050.

Sobolowski, S., G. Gong, and M. Ting, 2010: Modeled climate state and dynamic responses to anomalous North American snow cover. *J. Climate,* **23,** 785–799.

Thompson, D. W. J., and J. M. Wallace, 1998: The Arctic Oscillation signature in the wintertime geopotential height and temperature fields. *Geophys. Res. Lett.,* **25,** 1297–1300.

——, and ——, 2000: Annular modes in the extratropical circulation. Part I: Month-to-month variability. *J. Climate,* **13,** 1000–1016.

Vavrus, S., 2007: The role of terrestrial snow cover in the climate system. *Climate Dyn.,* **29,** 73–88.

Wagner, A. J., 1973: The influence of average snow depth on monthly mean temperature anomaly. *Mon. Wea. Rev.,* **101,** 624–626.

Watanabe, M., and T. Nitta, 1998: Relative impacts of snow and sea surface temperature anomalies on an extreme phase in the winter atmospheric circulation. *J. Climate,* **11,** 2837–2857.

Wilks, D. S., 2006: *Statistical Methods in the Atmospheric Sciences*. Academic Press, 648 pp.

Woollings, T. J., A. J. Charlton-Perez, S. Ineson, A. G. Marshall, and G. Masato, 2010: Associations between stratospheric variability and tropospheric blocking. *J. Geophys. Res.,* **115,** D06108, doi:10.1029/2009JD012742.

Wu, Q., H. Hu, and L. Zhang, 2011: Observed influences of autumn–early winter Eurasian snow cover anomalies on the hemispheric PNA-like variability in winter. *J. Climate,* **24,** 2017–2023.